Television Frequency Interference in AMSR2 K-Band Measurements Over Reflective Surfaces

Xiaoxu Tian and Xiaolei Zou

***Abstract*—The Advanced Microwave Scanning Radiometer 2 (AMSR2) measurements at K-band channels are used for snow retrieval. However, television (TV) signals transmitted from DirecTV satellites at the K-band, if reflected by snow surfaces, could enter the antenna of AMSR2 to introduce errors in AMSR2 snow products. This letter investigates TV frequency interference (TFI) in AMSR2 K-band measurements over areas of land covered with snow. Since a necessary condition for TFI over land to occur is for AMSR2 measurements to have small glint angles, a principal component analysis algorithm constrained by TFI glint angles for TFI detection is thus developed in this letter. Using AMSR2 observations in January 2014, it is shown that TFI signals exist along the two 55° incident angle curves of DirecTV-11 and DirecTV-12, which are located around 44° N over the North American continent.**

***Index Terms*—Advanced Microwave Scanning Radiometer 2 (AMSR2), K-band channels, television frequency interference (TFI) over snow surface.**

I. Introduction

THE Advanced Microwave Scanning Radiometer 2 (AMSR2) is the only remote sensing instrument onboard the Global Change Observation Mission—Water 1 (GCOM-W1) satellite, which was successfully launched onto a sun-synchronous orbit at an altitude of 700 km on May 18, 2012. It crosses the equator at 1:30 P.M. of local time [1]–[4]. AMSR2 is the successor of the AMSR-E onboard the Aqua satellite, which stopped its operation in October 2011. AMSR2 inherited all 12 channels of AMSR-E and added two new C-band channels at 7.3 GHz. It is well known that a number of channels in microwave imagers, such as 6.925 (C-band) and 10.65 GHz (X-band) of AMSR2, suffer from radio-frequency interference (RFI) from active sensors over densely populated cities [5]–[10]. The RFI sources primarily consist of radars, radio communication devices, traffic control monitors, etc. Over oceans, the reflected television (TV) signals from geostationary satellites cause TV interference (TFI) in microwave radiance observations [11]–[13]. In Europe, the TFI are found in X-band channels because the TV signals in the region are transmitted at X-band frequencies. Over coastal ocean areas of North America, TFI mainly exists in imager observations at K-band channels since the TV signal sources transmitted by DirecTV-11 and DirecTV-12 are around a frequency of 18.7 GHz.

McKague *et al.* [14] investigated the possible interference by TV signals to observations of WindSat, AMSR-E, and SSMI. The accumulated maximum spectral differences between observations of channels at 18.7 GHz and those at 23.8 GHz showed that K-band channel observations over land are likely to be interfered by TV signals reflected from snow surfaces. Zou *et al.* [12] pointed out that, the TFI glint angle, i.e., the angle between the line-of-sight vector and the reflected TV signal vector, is a necessary condition for the interference to occur. This letter develops a TFI detection algorithm based on principal component analysis (PCA) with TFI glint angles as the constraint. Since TFI is caused by reflected TV signals, it is not correlated with natural emission from a snow-covered land surface. Based on this characteristic, the PCA can isolate the TFI from the observations even when obscured by snow. Numerical results are made with AMSR2 L1B observation data.

II. AMSR2 Characteristics

AMSR2 is a conical scanning microwave imager with a constant local incident angle of 55°. Compared with its predecessor AMSR-E, the diameter of the antenna is increased from 1.6 to 2 m for AMSR2 to make measurements at higher spatial resolutions than AMSR-E. AMSR2 has in total 14 channels, with their center frequencies located at the following seven different frequencies: 6.925, 7.3, 10.65, 18.7, 23.8, 36.5, and 89 GHz. Each frequency has two channels measuring radiation at horizontally and vertically polarized states. Except for two channels at 7.3 GHz, the other 12 channels are inherited from AMSR-E. The purpose of adding two new channels is for RFI mitigation of observations at C-band. The swath width of AMSR2 is 1450 km. Each scan cycle has 486 Earth-scene field of views (FOVs) in 89-GHz channels and 243 FOVs in lower frequency channels. GCOM-W1 orbits the Earth about 14 times a day. This allows AMSR2 onboard GCOM-W1 to scan a majority part of the Earth twice daily. The GCOM-W1 satellite has a 16-day repeating cycle. The spatial resolution of instantaneous FOV (IFOV) at different channels, the sampling interval, and the beamwidths can be found in Table I.

III. TFI Detection Algorithm

The U.S. is fully covered with TV signals at K-band frequencies from both DirecTV-11 at 99.2° W and DirecTV-12

Manuscript received April 6, 2016; revised June 5, 2016 and July 11, 2016; accepted July 22, 2016. Date of publication August 25, 2016; date of current version October 12, 2016. This work was supported in part by the National Oceanic and Atmospheric Administration (NOAA) through the Hurricane Forecast Improvement Program (HFIP) under Project NA15NWS4680002 and the NOAA Proving Ground and Risk Reduction Program under Project NA11OAR4320199. (*Corresponding author: Xiaolei Zou.*)

The authors are with the Earth System Science Interdisciplinary Center, University of Maryland, College Park, MD 20740-3823 USA (e-mail: xzou1@umd.edu).

Digital Object Identifier 10.1109/LGRS.2016.2598058

TABLE I
AMSR2 INSTRUMENT CHARACTERISTICS

Channel Frequency [GHz]	Band Width [MHz]	Beam Width [deg]	IFOV [km]	NEDT [K]	Sampling Interval [km]	Pol.
6.925	350	1.8	35×62	0.34	10	H/V
7.3	350	1.8	34×58	0.43		
10.65	100	1.2	24×42	0.7		
18.7	200	0.65	14×22	0.7		
23.8	400	0.75	15×26	0.6		
36.5	1000	0.35	7×12	0.7		
89.0	3000	0.15	3×5	1.2	5	

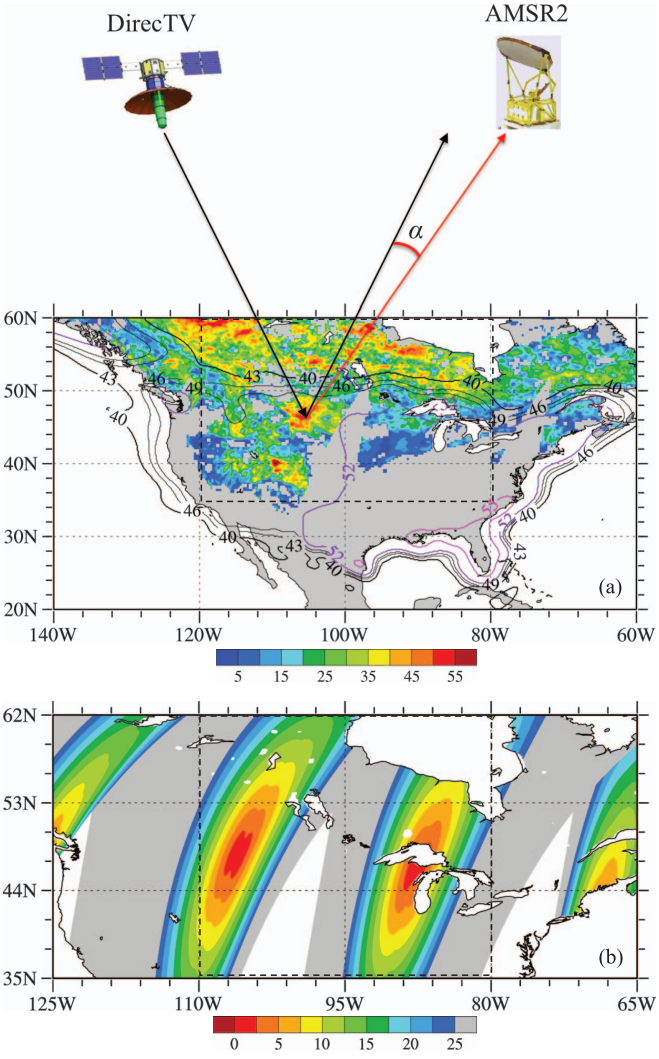

Fig. 1. (a) Schematic illustration of a potential occurrence of TFI over land, showing the AMSR2-retrieved snow depth (in centimeters, shaded in color) on January 5, 2014, and the coverage of DirecTV-12 with its signal intensity indicated in purple (55 dbW), light purple (52 dbW), and black contours (< 52 dbW) at 3-dbW interval. The symbol α represents the angle between a reflected TV signal vector (upward arrow in black) and AMSR2's scene vector (upward arrow in red). (b) Spatial distribution of α.

at 102.8° W. TV signals could be reflected and interfere with AMSR2 beam cones. Therefore, when AMSR2 is scanning the Earth's atmosphere to measure imager radiances over land in the U.S., it is possible that the TV signals reflected by snow

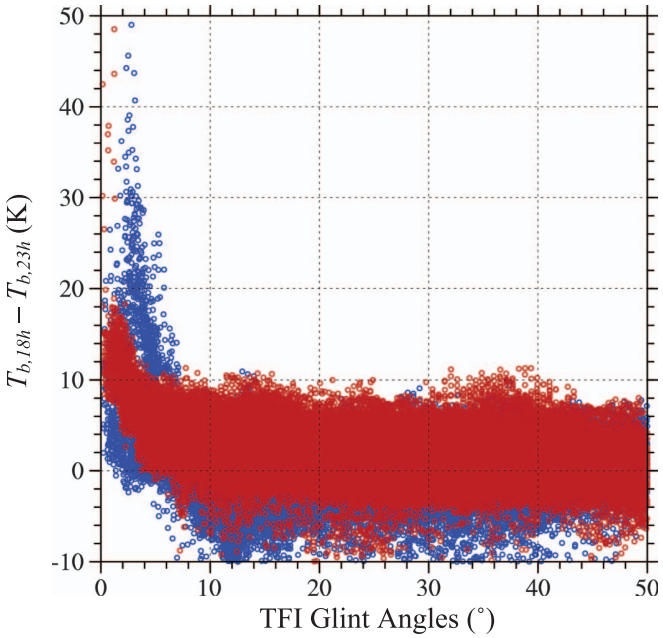

Fig. 2. Scatter plot of spectral difference distributions of brightness temperatures at horizontal polarizations of 18.7- and 23.8-GHz channels with respect to the TFI glint angles within the range in this figure on January 5, 2014. Data from the two swaths in this figure are colored in blue [east swath in the box of Fig. 1(b)] and red [west swath in the box of Fig. 1(b)], respectively.

surfaces can enter the antenna, which is similar to TFI over ocean [12], [13]. Fig. 1 provides a schematic illustration of a potential occurrence of TFI over land. It shows the AMSR2-retrieved snow depth on January 5, 2014, the coverage of DirecTV-12 with its signal intensity indicated [see Fig. 1(a)], and the angle between a reflected TV signal vector [see α, Fig. 1(b)] and AMSR2's scene vector. It is noticed that the DirecTV-12 signal intensity is strongest near the east coast. The signal intensity distribution from DirecTV-11 is similar to that of DirecTV-12 [13]. The symbol α refers to TFI glint angle. The smaller the TFI glint angle is, the more probable it is that the radiance observation can be interfered. Therefore, a small TFI glint angle is a necessary condition for TFI to occur. In addition to the glint angle, snow can also increase the spectral differences between low and high frequencies. Impacts of snow on radiative emission can only be detected at channels with frequencies greater than 20 GHz, which was the main principle for retrieving snow of a reasonable depth. The signal at 36.5 GHz can penetrate a shallow layer of snow. Therefore, a combination of 23.8 and 89 GHz channels can be applied to retrieve shallow snow depth to avoid the sensitivity of snow retrieval to shallow snow [15], [16].

If TV signals are reflected over snow surfaces and enter the antenna of AMSR2, the brightness temperatures at K-band channels (18.7 GHz) measured by AMSR2 would be warmer than those from natural radiation, whereas the brightness temperatures at 23.8-GHz channels are not affected by TFI. Fig. 2 shows the scatter plot of the same spectral difference with respect to TFI glint angles. It evidently indicates that the spectral difference values are abnormally high only when TFI glint angles are acute enough for the interference to enter AMSR2's antenna.

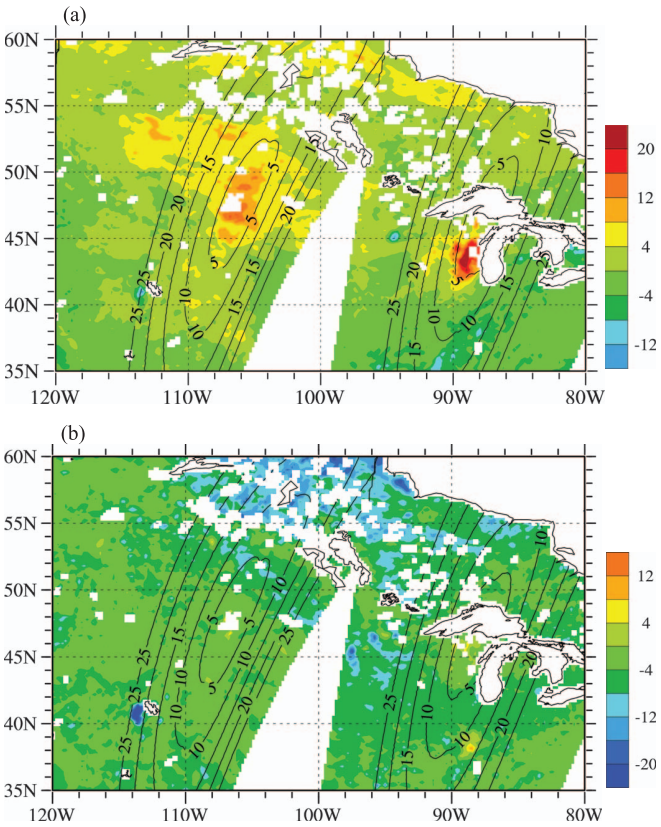

Fig. 3. Spectral difference (in kelvin) distributions of brightness temperatures at horizontal polarizations between 18.7- and 23.8-GHz channels (18.7 minus 23.8, shaded in color) and TFI glint angles (contoured for values less than 25°) on (a) January 5 and (b) August 17, 2014. Observations for AMSR2 pixels with land fractions being less than 90% are excluded to avoid lake effects on spectral differences.

The geographical distributions of differences of brightness-temperature observations at the horizontally polarized state between 18.7 GHz and those of 23.8 GHz on a winter snowing day (January 5) and a summer day (August 17) in 2014 are shown in Fig. 2. Since this paper focus on TFI over land, observations for AMSR2 pixels with land fractions being less than 90% are excluded in Fig. 3 to avoid lake effects on spectral differences, which can be significant in summer. The AMSR2 on these two days have the same swath distributions since the AMSR2's swath repeating time is 16 days. The TFI glint angle fields with respect to the geostationary TV satellites are also the same on January 5 and August 17, 2014. In Fig. 2(a), the two largest spectral differences of brightness-temperature observations between 18.7 GHz and those of 23.8 GHz are found west of Lake Michigan and the great plains of the U.S., where the TFI glint angles are small. These two areas are populated with snow [see Fig. 1(a)]. However, such large spectral differences of brightness-temperature observations between 18.7 GHz and 23.8 GHz are not found west of Lake Michigan and the great plains of the U.S. in the summer [see Fig. 2(b)], although the TFI glint angles are also small. It can thus be inferred that the K-band observations with snow coverage on January 5, 2014 could be TFI-contaminated in the aforementioned two areas. Compared with snow depth distribution shown in Fig. 1(a), it seems that the spectral differences between 18.7 and 23.8 GHz are positive and large over areas with large snow depth, which is expected due to larger scattering effects of snow at higher frequencies. However, the area characterized by the largest spectral differences between 18.7 and 23.8 GHz west of Lake Michigan has small snow depth. In other words, the TFI occurrence would increase the brightness temperatures of 18.7-GHz channels, and snow scattering would decrease the brightness temperatures at 23.8 GHz more significantly than at 18.7 GHz. Both TFI occurrence and snow reflection could increase the spectral differences between 18.7-GHz channels and 23.8-GHz channels. It is thus difficult to distinguish the effects of snow from the effects of TFI by simply examining the spectral differences between two different frequencies.

In order to isolate TFI from natural radiation over land with snow coverage, a spectral difference index vector $\text{Index}_{\text{TFI}-18H}$ is firstly defined for detecting TFI at 18.7 GHz at horizontal polarization. It consists of five spectral differences as its components

$$\text{Index}_{\text{TFI}-18H} = \begin{pmatrix} T_{b,18H} - T_{b,23H} \\ T_{b,10H} - T_{b,36H} \\ T_{b,10V} - T_{b,36V} \\ T_{b,23H} - T_{b,89H} \\ T_{b,23V} - T_{b,89V} \end{pmatrix}_{5\times 1} \tag{1}$$

where $\text{Index}_{\text{TFI}-18H}$ denotes the spectral difference index vector for 18.7-GHz H-Pol channel. All five components of the vector $\text{Index}_{\text{TFI}-18H}$ are related to Earth-surface-type information, such as snow, but TFI only exists in the first component of the vector. A data matrix is constructed from $\text{Index}_{\text{TFI}-18H}$ as follows:

$$\mathbf{A}_{5\times N} = (\text{Index}_{18H,1}\ \text{Index}_{18H,2}\ \cdots\ \text{Index}_{18H,N})_{5\times N} \tag{2}$$

where N is the total number of observation pixels over land with TFI glint angles less than 25°. The TFI glint angle threshold is set to 25° to ensure that all interfered observations are included (see Fig. 2). The covariance matrix $\mathbf{R}_{5\times 5}$ can be given by $\mathbf{R}_{5\times 5} = \mathbf{A}\mathbf{A}^T$. The eigenvalues and eigenvectors of the covariance matrix can then be obtained by solving the following:

$$\mathbf{R}\mathbf{e}_i = \lambda_i \mathbf{e}_i \tag{3}$$

where λ_i is the ith eigenvalue and $\mathbf{e}_i = [e_{1,i}, e_{2,i}, \ldots, e_{5,i}]$ is the ith principal component (PC) mode of $\mathbf{R}_{5\times 5}$. The ith eigenvalue λ_i quantifies the ith greatest variance contribution of the ith PC mode in the total variance of the data matrix $\mathbf{A}$. A set of PC coefficients $\mathbf{u}_i$ can be derived by projecting the original data matrix $\mathbf{A}$ onto the orthogonal space spanned by the eigenvectors $\mathbf{e}_i$

$$\begin{pmatrix} \mathbf{u}_1 \\ \mathbf{u}_2 \\ \vdots \\ \mathbf{u}_5 \end{pmatrix} = \mathbf{E}^T\mathbf{A}. \tag{4}$$

The original data matrix defined in (3) can be exactly reconstructed with the PC coefficients and PC modes in the following:

$$\mathbf{A} = \sum_{i=1}^{5} \mathbf{A}_i, \quad \text{where } \mathbf{A}_i = \mathbf{e}_i\mathbf{u}_i \tag{5}$$

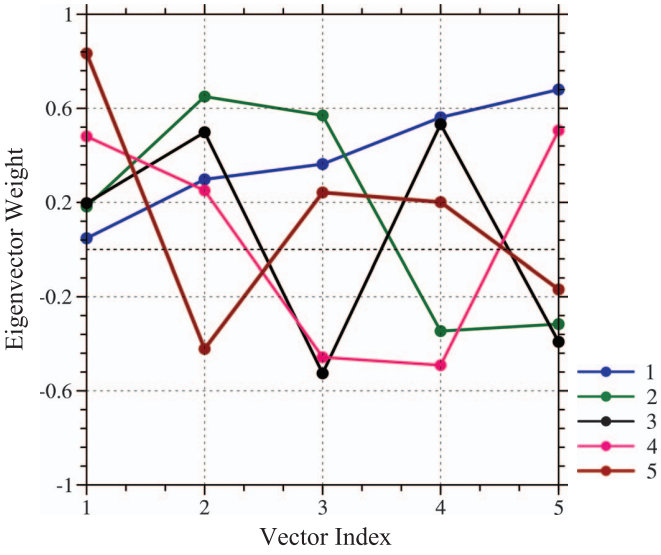

Fig. 4. Five PC modes (or eigenvectors) calculated in the PCA of spectral-difference distributions of brightness temperatures at horizontal polarizations of 18.7- and 23.8-GHz channels for the swath passing through 110 W in Fig. 2(a).

in (5) where $\mathbf{A}_i$ is the ith component accounting for the ith greatest variance in the original data matrix. Fig. 4 gives the eigenvectors yielded in the PCA for the data matrix composed with vectors defined in (1). It is noticed that the first component of the fifth eigenvector, i.e., $\mathrm{I}_{18H}^{\mathbf{A}_5} = (T_{b,18H} - T_{b,23H})^{\mathbf{A}_5}$, has the greatest value, reflecting a presence of TFI in the first component of the fifth eigenvector. Therefore, a new TFI intensity index over land with snow coverage is finally defined as

$$I_{\mathrm{TFI}-18H,\mathrm{snow}} = (T_{b,18H} - T_{b,23H})^{\mathbf{A}_5}. \tag{6}$$

IV. Numerical Results

The spatial distribution of $I_{\mathrm{TFI}-18H,\mathrm{snow}}$ for the AMSR2 observations in a typical snowing winter day is shown in Fig. 5. The large values of $I_{\mathrm{TFI}-18H,\mathrm{snow}}$ are found only over areas of west of Lake Michigan, the great plain with snow coverage, and small TFI glint angles. Other areas with large spectral differences of brightness temperatures between 18.7 GHz and 23.8 GHz shown in Fig. 3 are characterized with low TFI intensities. The TFI affected AMSR2 observations over snow surfaces are identified by the glint-angle constrained PCA algorithm.

The TFI glint angles are determined by both the differences of zenith and azimuth angles between the reflected TV signal vectors from the geostationary satellite and the Earth scene vectors of AMSR2. AMSR2 is a conical scanner with a fixed local incident angle of 55°. The angles of reflected TV signals are the same as those of the TV signals from DirecTV satellites. While the TV signal sources, i.e., the geostationary DirecTV satellites, are fixed with respect to the Earth, the incident angles for TV signals vary with respect to geographical locations. Only when the incident angles of TV signal vectors are close to 55° that the TFI glint angles approach zero. The TFI of AMSR2 observations would be most likely take place when TFI glint angles approach zero. To confirm this, we show in Fig. 6 a

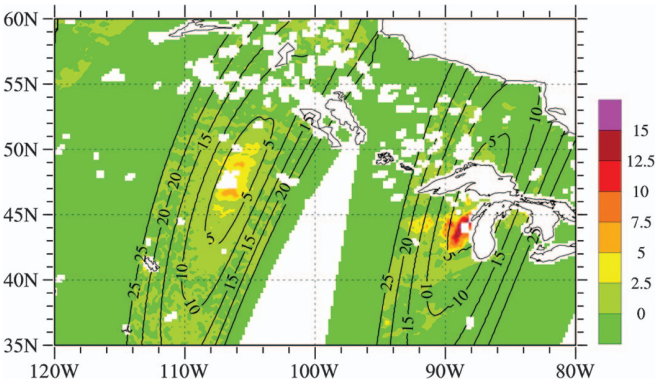

Fig. 5. TFI signal intensity (K) detected with PCA method and TFI glint angles (contoured for values less than 25°) on (a) January 5, and (b) August 17, 2014.

monthly distribution of the maximum TFI intensity in January 2014. The 55° incident angle of TV signals from DirecTV-11 and DirecTV-12 are indicated by the dashed and solid black curves, respectively. Within the one-month period, TFI over land by snow reflection is found in a latitudinal band following the two 55° incident angle curves of DirecTV-11 and Direct-12, extending from west to east coasts. The largest TFI is found near the east coast, where the intensity of TV signals is the strongest [see Fig. 1(a)].

V. Summary and Conclusions

Observations of microwave imagers at K-band channels, such as AMSR2, are of significant values for snow and ice retrievals. Before these imager observations are applied for geophysical product retrievals, the TFI affected observations have to be identified and removed. Otherwise, erroneous information in AMSR2 observations associated with TFI signals can be introduced into retrieval products. TFI at K-band channels over ocean was investigated by numerous previous studies. Since the reflectivity of snow is greater than that of bare land, TV signals from TV geostationary satellites can also be reflected back to space and enter the antenna of microwave radiometers. This letter investigated the K-band channel TFI over land with snow coverage and developed a PCA-based algorithm with TFI glint angles as a constraint. Over North America, TFI signals only exist at K-band channels and bring no correlations with other channels at different frequencies. The natural emissions measured at different frequencies are correlated—even under snowy conditions. A new PCA method is developed for TFI detection over snow-covered land.

Small angles between the reflected TV signal vectors and Earth scene vectors of radiometers are necessary conditions for TFI. The conical scan feature of AMSR2 determines that most TFI would occur over areas where the incident angles of TV signals from the geostationary satellites are close to the incident angles of AMSR2. The monthly maximum TFI distribution results from the proposed PCA detection algorithm confirmed this theoretical expectation. All TFI throughout the month are confined within the areas near the 55° incident angle curves of DirecTV-11 and DirecTV-12.

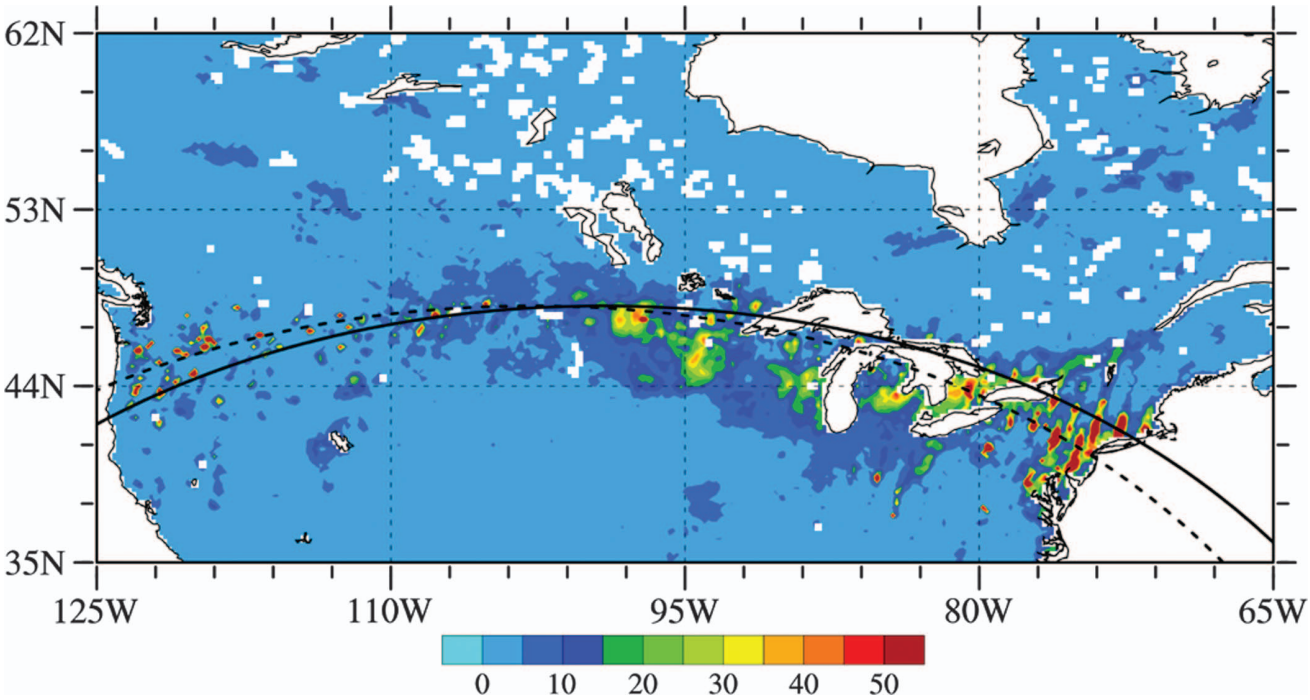

Fig. 6. Maximum TFI intensity (K) distribution in $1^\circ \times 1^\circ$ grid boxes for all the data in January of 2014 (shaded). The 55° incident angle lines of DirecTV-11 and Direct-12 are indicated by the dashed and solid black curves, respectively.

ACKNOWLEDGMENT

The authors would like to thank the Japan Aerospace Exploration Agency (JAXA) for providing AMSR-2 L1B observation data.

REFERENCES

[1] K. Imaoka *et al.*, "Five years of AMSR-E monitoring and successive GCOM-W1/AMSR2 instrument," *Proc. SPIE, Sens., Syst., Next-Generation Satellites XI*, 2007, vol. 6744, Art. no. 67440J, doi: 10.1117/12.740366.

[2] M. Kachi *et al.*, "Long-term observations of water and climate by AMSR-E and GCOM-W. Sensors, systems, and next-generation satellites XIII," *Proc. SPIE*, 2009, vol. 7474, pp. 1–9, doi: 10.1117/12.831253.

[3] K. Imaoka, M. Kachi, M. Kasahara, N. Ito, K. Nakagawa, and T. Oki, "Instrument performance and calibration of AMSR-E and AMSR2," in *Proc. Int. Archives Photogramm., Remote Sens. Spatial Inf. Sci.*, 2010, vol. 38, pp. 13–16.

[4] K. Imaoka *et al.*, "Status of AMSR2 instrument on GCOM-W1," in *Proc. SPIE*, 2012, vol. 8528, p. 15, doi: 10.1117/12.977774.

[5] L. Li, E. Njoku, E. Im, P. Chang, and K. S. Germain, "A preliminary survey of radio-frequency interference over the U.S. in Aqua AMSR-E data," *IEEE Trans. Geosci. Remote Sens.*, vol. 42, no. 2, pp. 380–390, Feb. 2004.

[6] E. Njoku, P. Ashcroft, T. Chan, and L. Li, "Global survey and statistics of radio-frequency interference in AMSR-E land observations," *IEEE Trans. Geosci. Remote Sens.*, vol. 43, no. 5, pp. 938–947, May 2005.

[7] L. Li, P. W. Gaiser, M. Bettenhausen, and W. Johnston, "WindSat radio-frequency interference signature and its identification over land and ocean," *IEEE Trans. Geosci. Remote Sens.*, vol. 44, no. 3, pp. 530–539, Mar. 2006.

[8] X. Zou, J. Zhao, F. Weng, and Z. Qin, "Detection of radio-frequency interference signal over land from FY-3B Microwave Radiation Imager (MWRI)," *IEEE Trans. Geosci. Remote Sens.*, vol. 50, no. 12, pp. 4994–5003, Dec. 2012.

[9] J. Zhao, X. Zou, and F. Weng, "WindSat radio-frequency interference signature and its identification over greenland and antarctic," *IEEE Trans. Geosci. Remote Sens.*, vol. 51, no. 9, pp. 4830–4839, Sep. 2013.

[10] D. Truesdale, "A probability distribution method for detecting radio-frequency interference in WindSat observations," *IEEE Trans. Geosci. Remote Sens.*, vol. 51, no. 6, pp. 3780–3788, Jun. 2013.

[11] I. S. Adams, M. H. Bettenhausen, P. W. Gaiser, and W. Johnston, "Identification of ocean-reflected radio frequency interference using WindSat retrieval chi-square probability," *IEEE Geosci. Remote Sens. Lett.*, vol. 7, no. 2, pp. 406–410, Apr. 2010.

[12] X. Zou, X. Tian, and F. Weng, "Detection of television frequency interference with satellite microwave imager observations over oceans," *J. Atmos. Ocean. Technol.*, vol. 31, pp. 2759–2776, 2014.

[13] X. Tian and X. Zou, "An empirical model for television frequency interference correction of AMSR2 data over ocean near the U.S. and Europe," *IEEE Trans. Geosci. Remote Sens.*, vol. 54, no. 7, pp. 3856–3867, Jul. 2016.

[14] D. McKague, J. J. Puckett, and C. Ruf, "Characterization of K-band radio frequency interference from AMSR-E, WindSat and SSM/I," in *Proc. IGARSS*, 2010, pp. 2492–2494.

[15] R. Kelly and A. T. C. Chang, "Development of a passive microwave global snow depth retrieval algorithm for Special Sensor Microwave Imager (SSM/I) and Advanced Microwave Scanning Radiometer-EOS (AMSR-E) data," *Radio Sci.*, vol. 38, p. 8076, 2003.

[16] R. Kelly, "The AMSR-E snow depth algorithm: Description and initial results," *J. Remote Sens. Soc. Jpn.*, vol. 29, no. 1, pp. 307–317, 2009.